ACS APPLIED MATERIALS & INTERFACES

Research Article

www.acsami.org

Tuning Micropillar Tapering for Optimal Friction Performance of Thermoplastic Gecko-Inspired Adhesive

Yongkwan Kim, Yunsie Chung, Angela Tsao, and Roya Maboudian*

Department of Chemical and Biomolecular Engineering, University of California, Berkeley, California 94720, United States

Supporting Information

ABSTRACT: We present a fabrication method and friction testing of a gecko-inspired thermoplastic micropillar array with control over the tapering angle of the pillar sidewall. A combination of deep reactive ion etching of vertical silicon pillars and subsequent maskless chemical etching produces templates with various widths and degrees of taper, which are then replicated with low-density polyethylene. As the silicon pillars on the template are chemically etched in a bath consisting of hydrofluoric acid, nitric acid, and acetic acid (HNA), the pillars are progressively thinned, then shortened. The replicated polyethylene pillar arrays exhibit a corresponding increase in friction as the stiffness is reduced with thinning and then a decrease in friction as the stiffness is again increased. The dilution of the HNA bath in water influences the tapering angle of the silicon pillars. The friction of the replicated pillars is maximized for the taper angle that maximizes the contact area at the tip which in turn is influenced by the stiffness of the tapered pillars. To provide insights on how changes in microscale geometry and contact behavior may affect friction of the pillar array, the pillars are imaged by scanning electron microscopy after friction testing, and the observed deformation behavior from shearing is related to the magnitude of the macroscale friction values. It is shown that the tapering angle critically changes the pillar compliance and the available contact area. Simple finite element modeling calculations are performed to support that the observed deformation is consistent with what is expected from a mechanical analysis. We conclude that friction can be maximized via proper pillar tapering with low stiffness that still maintains enough contact area to ensure high adhesion.

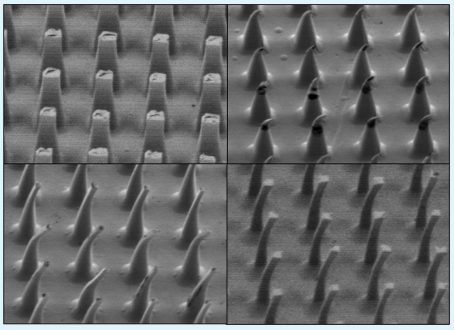

KEYWORDS: *gecko adhesives, micropillars, tapering, thermoplastics, silicon chemical etching*

INTRODUCTION

The adhesive foot-pads of geckos have attracted wide research interest in both understanding fibrillar attachment systems[1−4] and mimicking the micro- and nanoscale structures to engineer synthetic gecko adhesives.[5−12] Aided by developments in lithographic techniques, there has been impressive progress over the last decade in producing increasingly complex fiber structures that exhibit various aspects of gecko adhesion such as high adhesion/friction performance, reversible and directional attachment, and wet/dry self-cleaning.[5−12]

Not surprisingly, the attachment behavior of synthetic adhesive is very sensitive to the geometric parameters of the micro- and nanostructures that compose the fibrillar surfaces. Factors such as fiber aspect ratio,[13−18] tilting angle,[19−27] tip shape,[28−33] and hierarchy[34−48] influence the mechanical behavior of the individual fibers, which in turn have dramatic effects on their adhesion and friction behavior. As many synthetic gecko adhesives are high-aspect-ratio elastomer or thermoplastic, fabrication techniques rely on molding from either lithographically defined hard templates or soft lithography techniques that manipulate the shape of the resulting fibers.[5−12] One geometric aspect that has been difficult to control by either method and has not received much attention is the sidewall tapering of the fibers. While some wedge-shaped structures have been fabricated and tested for adhesive property, demonstrating several aspects of gecko adhesion (e.g., high ratio of detachment force to preload and nonadhesive default state),[49,50] the effect of the sidewall taper has not been studied in detail. Tuning the tapering angle of synthetic gecko adhesives could be useful for optimizing adhesion and friction performance of such adhesives as well as for exploring varied contact mechanisms dependent on the shape of the structure.

To this end, the present study introduces a technique for precise control over the sidewall tapering of silicon micropillars, which is then replicated by a thermoplastic to investigate the effect of pillar tapering on macroscale friction. A combination of deep reactive ion etching and chemical etching produces high aspect ratio silicon pillars with tunable tapering angle, depending on the chemical etching bath composition and the etching duration. A subsequent molding process replicates the structures in low-density polyethylene (LDPE) pillars, and their frictional behavior is studied and related to the pillar geometry. We report that the tapering angle can dramatically affect the contact mechanism of the pillars and the friction performance of the array, as a result of changes in the pillar compliance and

Received: February 4, 2014
Accepted: April 25, 2014
Published: April 25, 2014

   dx.doi.org/10.1021/am5007518 | ACS Appl. Mater. Interfaces 2014, 6, 6936−6943

the available contact area. Contact deformation of the pillars are imaged after friction testing by scanning electron microscopy (SEM) and compared with results from simple finite element models to provide insights into the observed friction behavior.

EXPERIMENTAL SECTION

Fabrication of Tapered Square Pillars. The overview for the fabrication of the tapered square pillar array is shown in Figure 1. The process begins by defining an array of pillars with

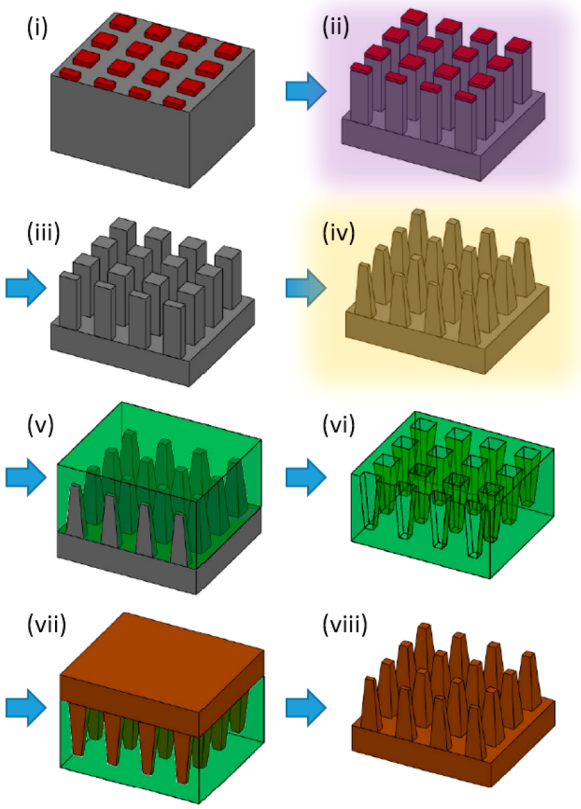

Figure 1. Process overview for the fabrication of tapered silicon pillar templates and their replication into LDPE thermoplastic, consisting of (i) photoresist patterning, (ii) deep reactive ion etching, (iii) photoresist removal, (iv) HNA etching, (v) polycarbonate film molding, (vi) intermediate template peel-off, (vii) LDPE film molding, and (viii) dissolution of the intermediate template in methylene chloride.

square cross sections via a photolithography process, in which a 4 in. Si(100) wafer is coated with a positive photoresist (Fujifilm, OCG 825) and light exposed (GCA 6200 – USH-350DP), using a photomask (Figure 1i). In place of a conventional mask patterned by electron beam lithography, a 100 nm thick layer of chromium is evaporated (Thermionics VE-100) through a plastic mesh (McMaster-Carr) onto a blank photomask, providing a cost-effective way to pattern a large area with an array of squares. The exposed wafer is developed, hard-baked, and etched by deep reactive ion etching (DRIE) employing an alternating pulse of SF_6 and C_4F_8 gases (STS2MPX ICP SR) to produce a vertical pillar array (Figure 1ii). The photoresist layer is subsequently removed by oxygen plasma (Figure 1iii). The processed wafer is diced into 1 × 1 cm^2 chips.

The pillars are then submerged in a silicon etch bath (Figure 1iv) consisting of hydrofluoric acid (EMD, 48%), nitric acid (EMD, 70%), and acetic acid (EMD, 99.7%). Even without any chemical etch mask, the resulting pillar shape could be controlled simply by diluting the etching bath with deionized water. The acids are first mixed in a volume ratio of 4:3:3 hydrofluoric/nitric/acetic acid (HNA). Each chip is exposed to 5 mL of the HNA solution diluted by an additional amount of water (in the range of 0−1 mL). When the chip is submerged in the bath, the reaction proceeds to etch away the pillars from the sides and the top, producing various angles of tapering and aspect ratios depending on the amount of dilution and the duration of etching. For most cases, the etching is fast, with the time staying under 1 min. Cross-sectional SEM (Agilent NovelX-MySEM) images of the templates are taken after cleaving them. Relevant pillar dimensions are measured from the SEM images with an image processing software (ImageJ 1.45s).

The resulting array of silicon pillars is replicated into a thermoplastic by a two-step molding process. To facilitate the peel-off, each silicon template is first coated with a self-assembled monolayer by a reaction with octadecyltrichlorosilane in toluene (in 1:1000 volume ratio).[51] Polycarbonate film (McMaster-Carr, 100 μm thick) is melted onto the silicon template in a vacuum oven at 300 °C for 1.5 h (Figure 1v), and the film is peeled-off after cooling (Figure 1vi). When a clean peel-off is not possible, the template is completely etched away with undiluted HNA solution. The intermediate polycarbonate template is used for molding LDPE film (McMaster-Carr, 100 μm) at 160 °C for 1 h (Figure 1vii), and the polycarbonate is dissolved away in methylene chloride (Figure 1viii).[51]

Friction Testing Procedure. Macroscale friction of each sample is measured using a standard pulley setup.[13] A 1 × 1 cm^2 patch is set on top of a smooth glass slide (Fisher Scientific) and pressed with 0.1 N of normal load. Weight is progressively added over a pulley, until the sample detaches from the glass. The glass slide is cleaned with acetone after each testing. Over multiple testing cycles with one sample, thermoplastic fiber arrays typically exhibit increasing friction initially (usually over 3 to 5 cycles) due to fiber and film alignment, then decreasing friction after the peak friction has been reached due to sample degradation and contamination. For each sample, the highest friction is the friction value reported for consistency. The error bars for the data presented are one standard deviation based on at least three different samples. The error in friction is likely due to some inconsistencies in fabrication, such as variation in silicon etching rates in DRIE and HNA steps, sample size, and sample quality, as well as measurement errors during the friction tests. After the friction testing, the samples are coated with Au/Pd (Hummer Sputtering System), and SEM images are taken to examine the state of the pillars. See Supporting Information Figure S1 for details on the friction testing setup.

Finite Element Modelling. For the finite element modelling (FEM), the pillar dimensions are first measured from SEM images of the fabricated LDPE pillars. For tapered shapes, height and two widths (top and bottom) are measured. Where the taper angle is reversed along the pillar length, the widths at the top, middle (thinnest part), and bottom are measured. The measured dimensions are used to construct a simplified geometry in ANSYS (Workbench 14.5.7). As boundary conditions, the bottom of the pillar, which is connected to the backing layer, is set fixed, and the top of

the pillar is loaded with a force in the direction parallel to the backing. The resulting total deformation from the original position is calculated. See Supporting Information Figure S2 for details on FEM.

RESULTS AND DISCUSSION

Fabricated Silicon Templates. Before any chemical etching, the square pillars obtained by DRIE show no tapering (inset of Figure 2a). The pillar width and height are 10 and 30

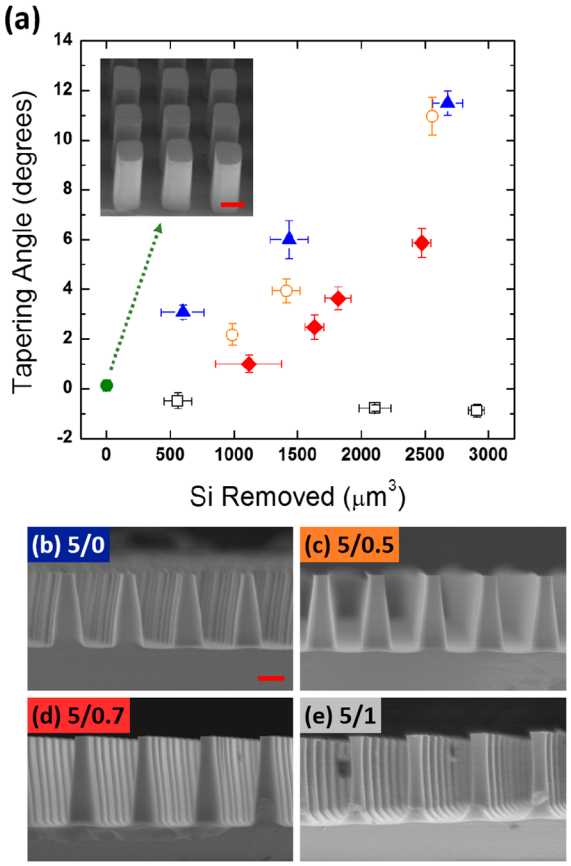

Figure 2. (a) Changes in tapering angle of silicon micropillars as etching reaction in HNA progresses at different dilution amounts by water (filled triangle = HNA/H_2O = 5:0 ratio by volume, empty circle = 5:0.5, filled diamond = 5:0.7, empty square = 5:1). The filled-circle data point corresponds to the original silicon pillars with no HNA etching (cross-sectional SEM image shown in the inset). Sample size 1 × 1 cm^2. Cross-sectional SEM images of silicon pillars etched in (b) 5:0 for 1 s, (c) 5:0.5 for 3 s, (d) 5:0.7 for 5 s, and (e) 5:1 for 15 s silicon templates. Scale bar = 10 μm.

μm, respectively, and the spacing between the pillars is 10 μm, corresponding to 250 000 pillar elements in a 1 × 1 cm^2 area. As described in the Experimental Section, the square pillars become tapered by exposure to a silicon etchant containing hydrofluoric, nitric, and acetic acids. This is an electrochemical reaction in which silicon is oxidized and subsequently dissolved by hydrofluoric acid with corresponding reduction of nitric acid,[52] resulting in an isotropic etching of silicon in contact with the solution. Acetic acid is commonly added to this process for moderating the reaction rate.[53] For this study, we have fixed the reagent ratio in HNA at 4:3:3 by volume adding up to the total of 5 mL for each 1 × 1 cm^2 chip. The HNA solution is diluted by various amounts (0−1 mL) of deionized water for further control over the etched structure, and the resulting etch bath is abbreviated by the volume ratio HNA/H_2O (in the range of 5:0 to 5:1). Figure 2 shows silicon templates after HNA etching at various dilutions. After only a few seconds of etching in undiluted HNA solution (5:0), the pillars are severely tapered (Figure 2b). Slight dilution by water (5:0.5) produces pillars with less severe tapering (Figure 2c), and the etching rate is slowed (see Supporting Information S3 for the effect of dilution on the etching rate). Etching in 5:0.7 condition further moderates the tapering (Figure 2d), and the 5:1 condition even shows slight reverse tapering (Figure 2e).

For a more comprehensive overview of the tapering development during etching, Figure 2a plots the angles estimated from the SEM images at various stages of etching progression under each condition. The degrees of tapering for different etching conditions are compared with respect to the volume of silicon removed since this is directly proportional to the number of atoms removed and thus indicative of the reaction rate. The tapering is increased with increasing etch time for each dilution condition (more negative for the 5:1 condition, where slight reverse tapering is observed), and dilution has decreased the tapering overall. Before the flat top area erodes away, the change in the pillar length is small compared to the original pillar length. However, towards the end of etching when the flat top area (or the thinnest middle for the reverse tapered pillar) has been etched away, tapering increases rapidly to leave behind low aspect ratio pyramids, regardless of dilution. These latter points have been omitted, and only the approximately linear regime is shown.

While HNA solution has long been used as a silicon etchant,[53] recent studies have shown the fabrication of various silicon architectures in micrometer length scale, for example, pyramidal tips,[54] channels,[55] and needles,[56] where hardmask patterns are used to allow etching in selected regions. In contrast, it is interesting to note that the chemical etching in this study is a maskless process in which predefined pillars are exposed to etchant with no intentional masking and simply diluting the solution allows precise control of the resulting morphology of the silicon structure. It is likely that in the case of the highly concentrated HNA bath (without dilution) with its fast etching rate significant removal of silicon could occur near the upper portion of the pillars before the solution can progressively reach the lower portion of the pillars for complete wetting. In other words, the etching rate is relatively fast for the concentrated HNA in comparison to the diffusion rate of the solution into the microchannels between the pillars, leading to the observed tapering. As the HNA solution is diluted, the etching rate slows, resulting in less severe tapering, as reported. Slight reverse tapering at high dilution may be due to nonuniform reaction rate along the depth. Because HNA etching of silicon is a highly exothermic reaction,[57] temperature gradients may develop in the region between the pillars and result in relatively slower etching of the upper portion.

While the exact etching mechanism remains speculative at this point, this method has allowed the preparation of silicon templates with various pillar thicknesses and tapering angles, which can subsequently be used to mold a thermoplastic film. LDPE replicas have been molded from silicon templates exposed to a range of etching conditions. Dilution of water is varied from 0 to 1 mL, and the etching duration has been adjusted so that most of the silicon pillars are etched away for the longest duration under each dilution condition. Here forth, the corresponding LDPE replica will be referred to by the

etching condition of the silicon template, namely, the dilution and the etch time, 5:0, 1 s.

Friction Behavior of the Molded LDPE Pillar Array. Figure 3a plots the friction behavior of LDPE pillars molded

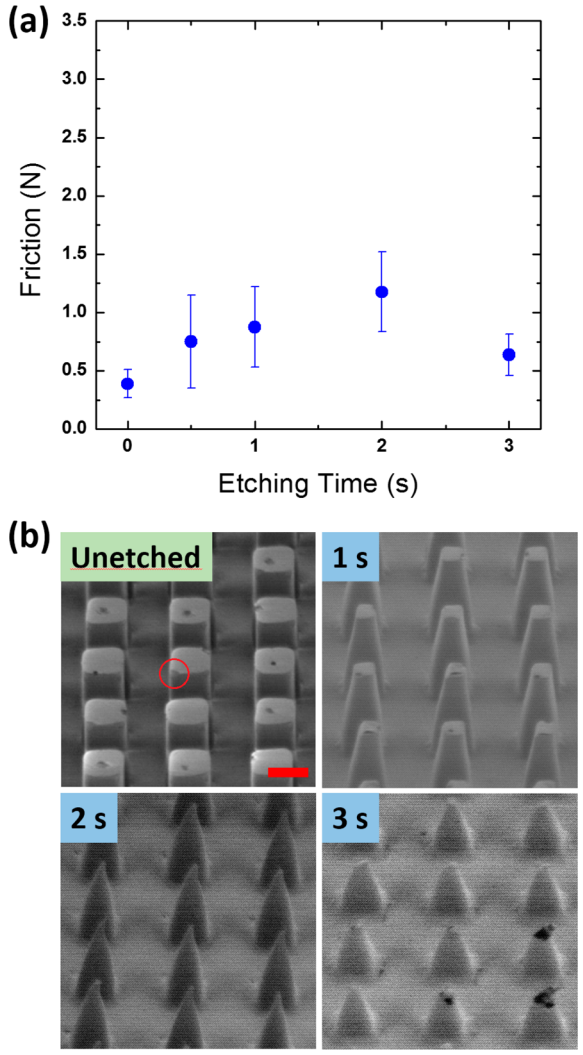

Figure 3. (a) Friction performance of the 1 × 1 cm^2 patch of the LDPE pillar array on smooth glass as template etching progresses in undiluted HNA solution (HNA/H_2O = 5:0 mL for each 1 × 1 cm^2 template). (b) Representative SEM images of LDPE pillars after friction testing for samples molded from unetched and 1, 2, and 3 s etched templates in 5:0 HNA/H_2O solution.

from Si templates etched with undiluted HNA solution (5:0). The friction force of 1 × 1 cm^2 unprocessed LDPE film against glass has been measured to be negligible (<0.1 N), while high friction (~10 N) has been measured when the LDPE film has been processed to be almost ideally flat by molding against a polished silicon wafer (this is expected since the contact area is maximized between two ideally flat surfaces). In comparison, the vertical LDPE pillars (Figure 3b, unetched) show minimal friction (0.4 N for the 1 × 1 cm^2 patch area, equivalent of holding about 40 g of weight). The corresponding SEM image after friction testing (Figure 3b, unetched) shows that some of the pillars have a corner that has been slightly flattened where the contact with glass has been made (some pits on top of the pillars are most likely air bubbles trapped during the molding step). It is likely that the contact is limited to the corner that first touches the counter-surface due to high stiffness of the pillar that prevents any significant bending to occur. As the template is progressively etched, the pillars are thinned, then shortened after the flat top area is etched away. There is a corresponding increase in friction of the LDPE replicas up to 1.2 N, followed by a decrease. As the template etching progresses, there is a corresponding thinning of the replicated LDPE pillars, and the contact has propagated to the entire edge with some of the pillars observed to have an edge that has plastically flowed over the top of the pillar (Figure 3b, 1 s). Further template etching has yielded sharp-tipped LDPE pillars (Figure 3b, 2 s) that appear to be bent only at the top. This deformation, however, is observed for all adjacent pillars, suggesting an increase in the number of contacting elements due to higher compliance of the thinned pillars.[13] Significantly shortened pillars (Figure 3b, 3s) with high stiffness are consistent with lower friction.

As the template etching bath is diluted (5:0.5), the tapering angle is moderated. The corresponding friction data of the replicated LDPE pillars are shown in Figure 4a, where a sharper increase in friction is observed in comparison to the 5:0 set. SEM images reveal that contact deformation occurred for most of the pillars even at the earlier stages of etching (Figure 4b, 1 and 3 s), where the plastically deformed edges are again observed at the top. Less severe tapering has led to pillars that are relatively more flexible due to thinning while preserving more of the tip area. This leads to both increased number of pillars in contacting glass as well as larger area of contact for each pillar, explaining why higher peak friction is observed for this set. Further etching has eliminated most of the tip area (Figure 4b, 5 s) and shows how tapering can be limiting to friction due to limited contact zone. While the thinner top area is seen to be deformed from contact, a thicker base prevents the deformation from propagating further. Later stages of etching again lead to shortening of the pillars (Figure 4b, 7 s), limiting the compliance and resulting in low friction. For the more diluted 5:0.7 case (see Figure S4, Supporting Information, for the SEM images and the friction data), the tapering is further moderated; the maximum friction has increased even further compared to the more tapered cases; and the higher friction is maintained over a larger range. In one particular case (5:0.7, 7 s), high friction is maintained despite having a very small top area. Here, a large bending deformation is observed over the entire pillar, and the sides have flattened on some of the pillars, suggesting that side contact has occurred. Side contact has been shown to increase contact zone,[58] and this could also be the case here where high friction was maintained despite significant reduction in contact area available at the tip.

Etching in 5:1 dilution leads to pillars that are slightly reverse tapered, with a thinner middle. A large increase in friction of the LDPE pillars is observed as template etching progresses (Figure 5a). While it is likely that the high friction is caused by the combination of increased pillar flexibility due to thinner middle and the large contact area preserved at the top, examination of SEM images for high friction samples (Figure 5b, 10, 15 s) reveals interesting differences from the previous tapered sets. The edge deformation is much less pronounced despite the high friction, suggesting that the stress has been more evenly distributed throughout the top during the shear loading. In particular, the 5:1, 15 s sample shows that significant bending has occurred but while maintaining the parallel contact with the counter-surface. By 20 s of etching, the top portion has been completely etched away, leaving residual wire structures in

dx.doi.org/10.1021/am5007518 | ACS Appl. Mater. Interfaces 2014, 6, 6936−6943

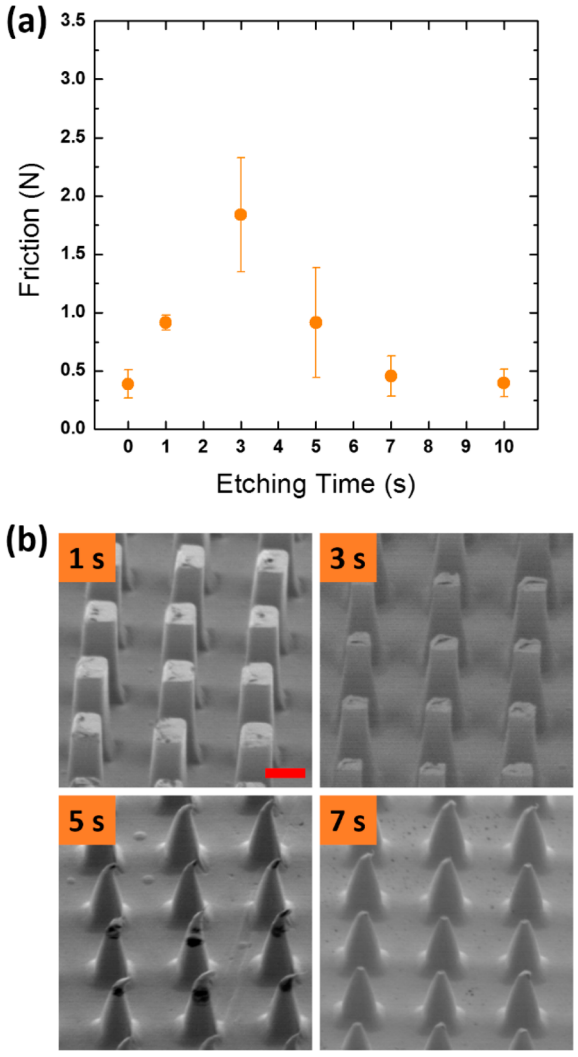

Figure 4. (a) Friction performance of the 1 × 1 cm^2 patch of the LDPE pillar array on smooth glass as template etching progresses in diluted HNA solution (HNA/H_2O = 5:0.5 mL for each 1 × 1 cm^2 template). (b) Representative SEM images of LDPE pillars after friction testing for samples molded from 1, 3, 5, and 7 s etched templates in 5:0.5 solution.

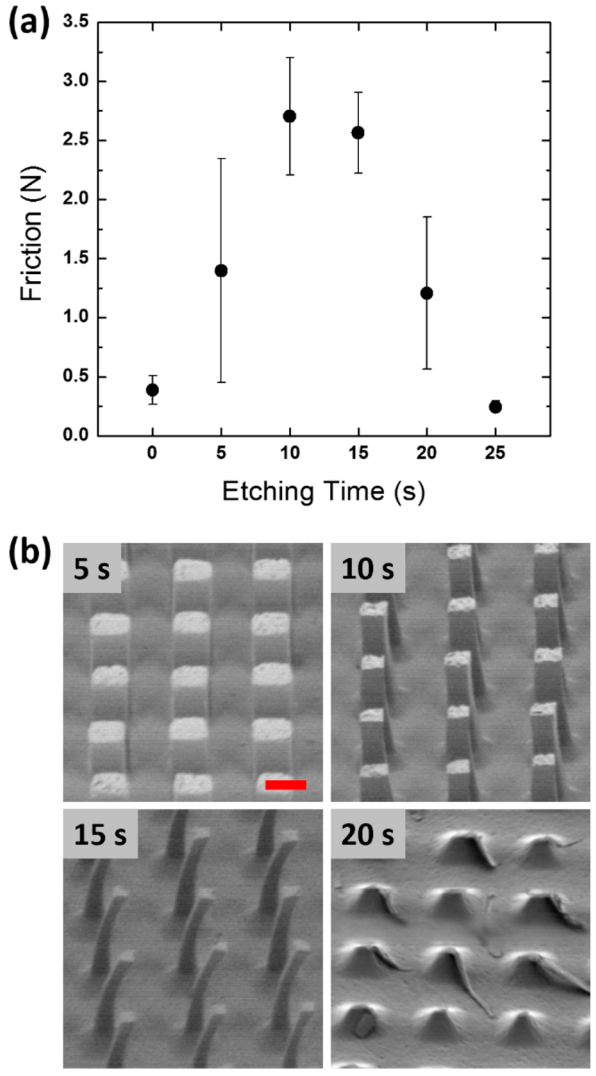

Figure 5. (a) Friction performance of the 1 × 1 cm^2 patch of the LDPE pillar array on smooth glass as template etching progresses in diluted HNA solution (HNA/H_2O = 5:1 mL for each 1 × 1 cm^2 template). (b) Representative SEM images of LDPE pillars after friction testing for samples molded from 5, 10, 15, and 20 s etched templates in 5:1 solution.

some parts that have collapsed as they are too thin to maintain structural integrity.

Comparing Observed Deformation Behavior with Finite Element Modelling. To provide further insight into the deformation observed after friction testing, we have performed finite element modelling for various pillar shapes. For simplicity, a perfectly square cross-section with linear tapering is assumed, and relevant dimensions are estimated from the SEM images. With a fixed boundary condition at the bottom of the pillar, a force of 10 μN is applied to the top surface in the direction parallel to the sample to see the initial stage of bending during shear loading (see Supporting Information Figure S2 for details). The applied force of 10 μN is an order of magnitude approximation from 1 N force (range observed from the friction data) distributed to 250 000 pillars on a 1 × 1 cm^2 area. This yields 4 μN/pillar, but the actual load on each pillar is likely much higher since not all pillars are in contact. This actual force would be dependent on the shape, but fixing the load at 10 μN allows a comparison of stiffness across all shapes. The resulting deformation in the cross-section through the middle of the pillar is shown in Figure 6 for four representative shapes. The deformation value indicates in micrometers the distance each point has moved from the original position. As the same load is applied to all pillars, larger deformation corresponds to relatively less stiff pillar geometry.

For the unetched shape (Figure 6a), a small deformation of ~0.58 μm is predicted at the tip. This is consistent with the SEM observation (Figure 3b, unetched), where no significant change in the structure has occurred other than occasional dents in some corners suggesting contact. It is likely that the high stiffness has prevented neighboring pillars from coming into contact, given unavoidable pillar-to-pillar height variation from fabrication. With a high degree of tapering (Figure 6b), the FEM suggests a large bending only at the top portion of the pillar, also consistent with experimentally observed behavior for pillars of similar shape (Figure 4b, 5 s). As most of the top area has been etched away, the pillar sides would have to come into contact to result in high friction. However, the stiff portion

dx.doi.org/10.1021/am5007518 | ACS Appl. Mater. Interfaces 2014, 6, 6936−6943

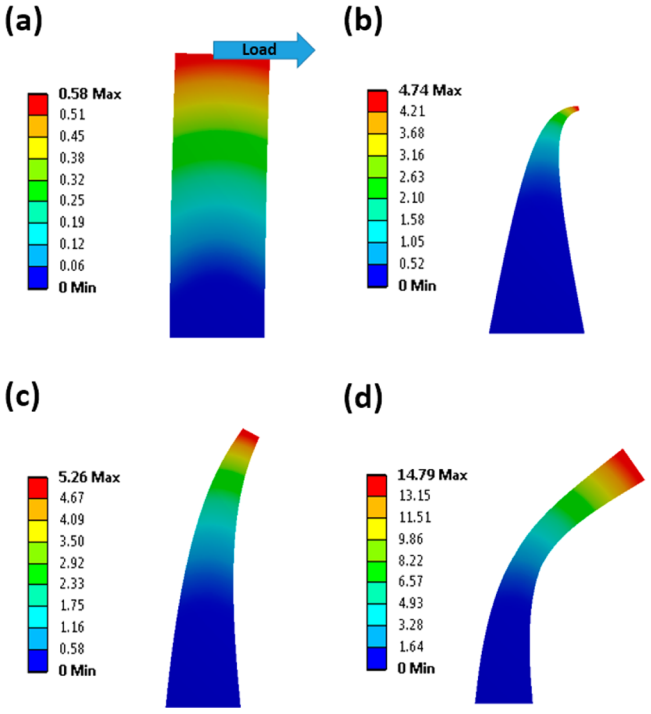

Figure 6. Bending behavior of various shaped pillars predicted by finite element modelling. Geometries are based on LDPE pillars molded from (a) unetched, (b) 5:0.5, 5 s, (c) 5:0.7, 7 s, and (d) 5:1, 15 s etched templates. Total deformation on a cross-sectioned plane down the middle is displayed with the maximum value in micrometers noted.

towards the base limits the bending and only allows the sides very close to the top to come into contact. With less severe tapering, deformation is propagated further down the pillar, resulting in greater deformation throughout the entire pillar (Figure 6c). This compliance of the whole pillar can allow other neighboring pillars to come into contact and also make side contact possible, as confirmed by the SEM images that show all pillars in the vicinity have been deformed and some have been flattened on the sides (Figure S4b, 7 s, Supporting Information). The reverse tapered shape (Figure 6d) is thinnest in the middle, and it is predicted that a large bending occurs there. However, this contact shape is different from that observed in the SEM images (Figure 5b, 15 s), where the top surface is still aligned parallel to the counter surface. It seems the large top contact area has ensured enough adhesion to prevent rotational bending of the pillar. Nonetheless, the thin middle portion still enables a high degree of deformation and thus allows a large number of pillars to contact the counter surface, and the large top area ensures enough adhesion is provided by each pillar. It is also noted that while the real area of contact created between a pillar and the glass is influenced by the shape of the pillar, it alone cannot fully account for the observed macroscale friction behavior. For example, the ratio of friction force to the area per fiber estimated from the deformed region of contact for the vertical pillars (Figure 3b, unetched) is 0.39 N/2.8 μm^2 = 0.14 N/μm^2. In comparison, the same analysis for 5:0.5, 5 s and 5:1, 15 s samples yields 0.3 and 0.28 N/μm^2 showing that the macroscale friction does not simply scale with the real contact area of each pillar. Stiffness must also be taken into account to consider the number of pillars that are in contact, in addition to the contact area of an individual pillar which is influenced by the top area of the structure.

To further examine the effect of pillar stiffness and contact area on the observed macroscale friction, the deformation predicted by ANSYS and top area of the pillar shapes estimated from the SEM images for the 5:0.5 etch condition have been plotted in Figure 7, along with the experimentally obtained

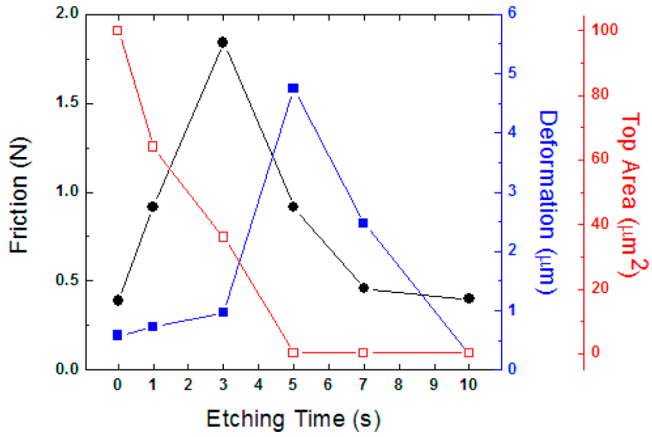

Figure 7. Experimentally obtained friction, total deformation (indicative of pillar stiffness), and top area change of the replicated LDPE pillars as the template etching progresses in 5:0.5 solution. Filled circle = friction, filled square = deformation, and empty square = top area. A maximum is observed in compliance, but the top area continuously decreases to near 0.

friction data. As expected, a dramatic decrease in stiffness (corresponding to higher deformation) is observed as pillars are thinned during etching, followed by an increase (corresponding to lower deformation) due to shortening once the top has been etched away. While it is reasonable that higher compliance enables a higher number of pillars in contact,[13,39] the peak value occurs at longer etching time than observed in the friction data (Figure 4a). Accounting for the eroding top area, however, it would shift the peak to lower values, closer to the friction result. Despite its simplicity, the analysis based on pillar deformation and available top area qualitatively captures key elements affected by the tapering angle: the tapered pillars should be compliant enough to ensure a large number of contacts, while sufficient contact area should be available on each pillar since the macroscale friction performance depends on the combination of the two factors.

CONCLUSION

We have presented a simple method for tuning the tapering angle of a silicon pillar array by maskless chemical etching of lithographically defined vertical pillars. While etching tapered, thinned, and then eventually shortened the pillars, dilution of the etching solution by water decreased the tapering angle of the resulting pillars. By using them as templates for molding, the thermoplastic pillar array with a variety of shapes could be fabricated. Frictional testing showed that the friction behavior of the film was very sensitive to the tapering angle. In general, friction initially increased with increasing etching time of the template as the pillars thinned to be more compliant but decreased as the top started to etch away and pillars were shortened. As tapering angle decreased, the peak friction value could be significantly increased. SEM observation of deformed pillars after testing revealed that the contact behavior was dependent on the pillar shape. In general, progressively etching the silicon template led to thinning of the pillars and then

dx.doi.org/10.1021/am5007518 | ACS Appl. Mater. Interfaces 2014, 6, 6936−6943

shortening of the pillars that led to a corresponding increase and decrease in compliance of the molded LDPE pillars. While thicker pillars molded from templates with short etching time showed little deformation due to high stiffness, highly tapered pillars showed contact deformation limited to the top portion of the pillar. As tapering angle decreased, deformation was more pronounced throughout the entire pillar. Simple finite element modelling confirmed that observed deformation is consistent with what was expected from mechanical analysis and provided useful insights into the contributing factors of pillar compliance and contact area. As template etching proceeds, there is an optimum in compliance; however, contact area continually decreases, and the resulting macroscale friction is a combined effect of the two. Decreasing tapering effectively leads to preserving the contact area available at the top as pillars are thinned for higher compliance.

■ ASSOCIATED CONTENT

Supporting Information

Details on the friction testing method, finite element modelling, and chemical etching reaction rate. This material is available free of charge via the Internet at http://pubs.acs.org.

■ AUTHOR INFORMATION

Corresponding Author

*E-mail: maboudia@berkeley.edu.

Notes

The authors declare no competing financial interest.

■ ACKNOWLEDGMENTS

This work was supported by the National Science Foundation grants EEC-0832819 (through the Center of Integrated Nanomechanical Systems) and DMR-0804646. Silicon templates were fabricated in the Marvell Nanofabrication Laboratory.

■ REFERENCES

(1) Autumn, K.; Liang, Y. A.; Hsieh, S. T.; Zesch, W.; Chan, W. P.; Kenny, T. W.; Fearing, R.; Full, R. J. Adhesive Force of a Single Gecko Foot-hair. *Nature* **2000**, *405*, 681−685.

(2) Autumn, K.; Sitti, M.; Liang, Y. A.; Peattie, A. M.; Hansen, W. R.; Sponberg, S.; Kenny, T. W.; Fearing, R.; Israelachvili, J. N.; Full, R. J. Evidence for van der Waals Adhesion in Gecko Setae. *Proc. Natl. Acad. Sci. U.S.A.* **2002**, *99*, 12252−12256.

(3) Arzt, E.; Gorb, S.; Spolenak, R. From Micro to Nano Contacts in Biological Attachment Devices. *Proc. Natl. Acad. Sci. U.S.A.* **2003**, *100*, 10603−10606.

(4) Tian, Y.; Pesika, N.; Zeng, H.; Rosenberg, K.; Zhao, B.; McGuiggan, P.; Autumn, K.; Israelachvili, J. Adhesion and Friction in Gecko Toe Attachment and Detachment. *Proc. Natl. Acad. Sci. U.S.A.* **2006**, *103*, 19320−19325.

(5) Boesel, L. F.; Greiner, C.; Arzt, E.; del Campo, A. Gecko-Inspired Surfaces: A Path to Strong and Reversible Dry Adhesives. *Adv. Mater.* **2010**, *22*, 2125−2137.

(6) Sameoto, D.; Menon, C. Recent Advances in the Fabrication and Adhesion Testing of Biomimetic Dry Adhesives. *Smart Mater. Struct.* **2010**, *19*, 103001.

(7) del Campo, A.; Arzt, E. Design Parameters and Current Fabrication Approaches for Developing Bioinspired Dry Adhesives. *Macromol. Biosci.* **2007**, *7*, 118−127.

(8) Jeong, H. E.; Suh, K. Y. Nanohairs and Nanotubes: Efficient Structural Elements for Gecko-Inspired Artificial Dry Adhesives. *Nano Today* **2009**, *4*, 335−346.

(9) Kwak, M. K.; Pang, C.; Jeong, H.; Kim, H.; Yoon, H.; Jung, H.; Suh, K. Towards the Next Level of Bioinspired Dry Adhesives: New Designs and Applications. *Adv. Funct. Mater.* **2011**, *21*, 3606−3616.

(10) Hu, S.; Xia, Z. Rational Design and Nanofabrication of Gecko-Inspired Fibrillar Adhesives. *Small* **2012**, *8*, 2464−2468.

(11) Jagoda, A.; Hui, C. Adhesion, Friction, and Compliance of Bio-mimetic and Bio-inspired Structured Interfaces. *Mater. Sci. Eng., R* **2011**, *72*, 253−292.

(12) Juan, L.; Qinglin, Y.; Jingjing, X.; Kesong, L.; Lin, G.; Lei, J. Adhesive Materials Inspired by Gecko and Mussel. *Prog. Chem.* **2012**, *24*, 1946−1954.

(13) Lee, D. H.; Kim, Y.; Fearing, R. S.; Maboudian, R. Effect of Fiber Geometry on Macroscale Friction of Ordered Low-Density Polyethylene Nanofiber Arrays. *Langmuir* **2011**, *27*, 11008−11016.

(14) Greiner, C.; del Campo, A.; Arzt, E. Adhesion of Bioinspired Micropatterned Surfaces: Effects of Pillar Radius, Aspect Ratio, and Preload. *Langmuir* **2007**, *23*, 3495−3502.

(15) Burton, Z.; Bhushan, B. Hydrophobicity, Adhesion, and Friction Properties of Nanopatterned Polymers and Scale Dependence for Micro- and Nanoelectromechanical Systems. *Nano Lett.* **2005**, *5*, 1607−1613.

(16) Qu, L.; Dai, L.; Stone, M.; Xia, Z.; Wang, Z. L. Carbon Nanotube Arrays with Strong Shear Binding-On and Easy Normal Lifting-Off. *Science* **2008**, *322*, 238−242.

(17) Glassmaker, N. J.; Jagota, A.; Hui, C. Adhesion Enhancement in a Biomimetic Fibrillar Interface. *Acta Biomater.* **2005**, *1*, 367−375.

(18) Zhao, Y.; Tong, T.; Delzeit, L.; Kashani, A.; Meyyappan, M.; Majumdar, A. Interfacial Energy and Strength of Multiwalled-Carbon-Nanotube-Based Dry Adhesive. *J. Vac. Sci. Technol. B* **2006**, *24*, 331−335.

(19) Aksak, B.; Murphy, M. P.; Sitti, M. Adhesion of Biologically Inspired Vertical and Angled Polymer Microfiber Arrays. *Langmuir* **2007**, *23*, 3322−3332.

(20) Kim, T.; Jeong, H. E.; Suh, K. Y.; Lee, H. H. Stooped Nanohairs: Geometry-Controllable, Unidirectional, Reversible, and Robust, Gecko-like Dry Adhesive. *Adv. Mater.* **2009**, *21*, 2276−2281.

(21) Yoon, H.; Jeong, H. E.; Kim, T.; Kang, T. J.; Tahk, D.; Char, K.; Suh, K. Y. Adhesion Hysteresis of Janus Nanopillars Fabricated by Nanomolding and Oblique Metal Deposition. *Nano Today* **2009**, *4*, 385−392.

(22) Moon, M.; Cha, T.; Lee, K.; Vaziri, A.; Kim, H. Tilted Janus Polymer Pillars. *Soft Matter* **2010**, *6*, 3924−3929.

(23) Lee, J.; Fearing, R. S.; Komvopoulos, K. Directional Adhesion of Gecko-Inspired Angled Microfiber Arrays. *Appl. Phys. Lett.* **2008**, *93*, 191910.

(24) Santos, D.; Spenko, M.; Parness, A.; Kim, S.; Cutkosky, M. Directional Adhesion for Climbing: Theoretical and Practical Considerations. *J. Adhes. Sci. Technol.* **2007**, *21*, 1317−1341.

(25) Murphy, M. P.; Aksak, B.; Sitti, M. Adhesion and Anisotropic Friction Enhancements of Angled Heterogeneous Micro-fiber Arrays with Spherical and Spatula Tips. *J. Adhes. Sci. Technol.* **2007**, *21*, 1281−1296.

(26) Jeong, H. E.; Lee, J.; Kwak, M. K.; Moon, S. H.; Suh, K. Y. Effect of Leaning Angle of Gecko-Inspired Slanted Polymer Nanohairs on Dry Adhesion. *Appl. Phys. Lett.* **2010**, *96*, 043704.

(27) Yu, J.; Chary, S.; Das, S.; Tamelier, J.; Pesika, N. S.; Turner, K. L.; Israelachvili, J. N. Gecko-Inspired Dry Adhesive for Robotic Applications. *Adv. Funct. Mater.* **2011**, *21*, 3010−3018.

(28) del Campo, A.; Greiner, C.; Álvaerez, I.; Arzt, E. Patterned Surfaces with Pillars with Controlled 3D Tip Geometry Mimicking Bioattachment Devices. *Adv. Mater.* **2007**, *19*, 1973−1977.

(29) del Campo, A.; Greiner, C.; Arzt, E. Contact Shape Controls Adhesion of Bioinspired Fibrillar Surfaces. *Langmuir* **2007**, *23*, 10235−10243.

(30) Kim, S.; Sitti, M. Biologically Inspired Polymer Microfibers with Spatulate Tips as Repeatable Fibrillar Adhesives. *Appl. Phys. Lett.* **2006**, *89*, 261911.

(31) Murphy, M. P.; Aksak, B.; Sitti, M. Gecko-Inspired Directional and Controllable Adhesion. *Small* **2009**, *5*, 170−175.

(32) Davies, J.; Haq, S.; Hawke, T.; Sargent, J. P. A Practical Approach to the Development of a Synthetic Gecko Tape. *Int. J. Adhes. Adhes.* **2009**, *29*, 380−390.
(33) Wang, D.; Zhao, A.; Jiang, R.; Li, D.; Zhang, M.; Gan, Z.; Tao, W.; Guo, H.; Mei, T. Surface Properties of Bionic Micro-pillar Arrays with Various Shapes of Tips. *Appl. Surf. Sci.* **2012**, *259*, 93−98.
(34) Murphy, M. P.; Kim, S.; Sitti, M. Enhanced Adhesion by Gecko-Inspired Hierarchical Fibrillar Adhesives. *ACS Appl. Mater. Interfaces* **2009**, *1*, 849−855.
(35) Jeong, H. E.; Lee, J.; Kim, H. N.; Moon, S. H.; Suh, K. Y. A Nontransferring Dry Adhesive with Hierarchical Polymer Nanohairs. *Proc. Natl. Acad. Sci. U.S.A.* **2009**, *106*, 5639−5644.
(36) Lee, J.; Bush, B.; Maboudian, R.; Fearing, R. S. Gecko-Inspired Combined Lamellar and Nanofibrillar Array for Adhesion on Nonplanar Surfaces. *Langmuir* **2009**, *25*, 12449−12453.
(37) Lee, H.; Bhushan, B. Fabrication and Characterization of Hierarchical Nanostructured Smart Adhesion Surfaces. *J. Colloid Interface Sci.* **2012**, *372*, 231−238.
(38) Hu, S.; Jiang, H.; Xia, Z.; Gao, X. Friction and Adhesion of Hierarchical Carbon Nanotube Structures for Biomimetic Dry Adhesives: Multiscale Modeling. *ACS Appl. Mater. Interfaces* **2010**, *2*, 2570−2578.
(39) Izadi, H.; Zhao, B.; Han, Y.; McManus, N.; Penlidis, A. Teflon Hierarchical Nanopillars with Dry and Wet Adhesive Properties. *J. Polym. Sci., Part B: Polym. Phys.* **2012**, *50*, 846−851.
(40) Greiner, C.; Arzt, E.; del Campo, A. Hierarchical Gecko-Like Adhesives. *Adv. Mater.* **2009**, *21*, 479−482.
(41) Huovinen, E.; Hirvi, J.; Suvanto, M.; Pakkanen, T. A. Micro-Micro Hierarchy Replacing Micro-Nano Hierarchy: A Precisely Controlled Way to Produce Wear-Resistant Superhydrophobic Polymer Surfaces. *Langmuir* **2012**, *28*, 14747−14755.
(42) Röhrig, M.; Thiel, M.; Worgull, M.; Hölscher, H. 3D Direct Laser Writing of Nano- and Microstructured Hierarchical Gecko-Mimicking Surfaces. *Small* **2012**, *8*, 3009−3015.
(43) Hu, S.; Xia, Z.; Gao, X. Strong Adhesion and Friction Coupling in Hierarchical Carbon Nanotube Arrays for Dry Adhesive Applications. *ACS Appl. Mater. Interface* **2012**, *4*, 1972−1980.
(44) Izadi, H.; Golmakani, M.; Penlidis, A. Enhanced Adhesion and Friction by Electrostatic Interactions of Double-level Teflon Nanopillars. *Soft Matter* **2013**, *9*, 1985−1996.
(45) Lee, D. Y.; Lee, D. H.; Lee, S. G.; Cho, K. Hierarchical Gecko-inspired Nanohairs with a High Aspect Ratio Induced by Nano-yielding. *Soft Matter* **2012**, *8*, 4905−4910.
(46) Zhang, H.; Wu, L.; Jia, S.; Guo, D.; Dai, Z. Fabrication and Adhesion of Hierarchical Micro-Seta. *Chin. Sci. Bull.* **2012**, *57*, 1343−1349.
(47) Ho, A. Y. Y.; Yeo, L. P.; Lam, Y. C. Rodríguez. Fabrication and Analysis of Gecko-Inspired Hierarchical Polymer Nanosetae. *ACS Nano* **2011**, *5*, 1897−1906.
(48) Zhang, P.; Liu, S.; Lv, H. Fabrication and Properties of Dual-Level Hierarchical Structures Mimicking Gecko Foot Hairs. *J. Nanosci. Nanotechnol.* **2013**, *13*, 781−786.
(49) Parness, A.; Soto, D.; Esparza, N.; Gravish, N.; Wilkinson, M.; Autumn, K.; Cutkosky, M. A Microfabricated Wedge-shaped Adhesive Array Displaying Gecko-like dynamic Adhesion, Directionality and Long Lifetime. *J. R. Soc. Interface* **2009**, *6*, 1223−1232.
(50) Chary, S.; Tamelier, J.; Turner, K. A Microfabricated Gecko-Inspired Controllable and Reusable Dry Adhesive. *Smart Mater. Struct.* **2013**, *22*, 025013.
(51) Kim, Y.; Limanto, F.; Lee, D. H.; Fearing, R. S.; Maboudian, R. Role of Counter-substrate Surface Energy in Macroscale Friction of Nanofiber Arrays. *Langmuir* **2012**, *28*, 2922−2927.
(52) Turner, D. R. On the Mechanism of Chemically Etching Germanium and Silicon. *J. Electrochem. Soc.* **1960**, *107*, 810−816.
(53) Schwartz, B.; Robbins, H. Chemical Etching of Silicon − IV. Etching Technology. *J. Electrochem. Soc.* **1976**, *123*, 1903−1909.
(54) Resnik, D.; Vrtacnik, D.; Aljancic, U.; Mozek, M.; Amon, S. Different Aspect Ratio Pyramidal Tips Obtained by Wet Etching. *Microelectron. J.* **2003**, *34*, 591−593.
(55) Bauhuber, M.; Mikrievskij, A.; Lechner, A. Isotropic Wet Chemical Etching of Deep Channels with Optical Surface Quality in Silicon with HNA Based Etching Solutions. *Mater. Sci. Semicond. Process* **2013**, *16*, 1428−1433.
(56) Hamzah, A. A.; Abd Aziz, N.; Yeop Majlis, B.; Yunas, J.; Dee, C. F.; Bais, B. Optimization of HNA Etching Parameters to Produce High Aspect Ratio Solid Silicon Microneedles. *J. Micromech. Microeng.* **2012**, *22*, 095017.
(57) Hui, W. How to Prevent Runaway Chemical Reaction in the Isotropic Etching of Silicon with $HF/HNO_3/CH_3COOH$ or HNA Solution. *Proc. SPIE* **2004**, *5276*, 270−279.
(58) Lee, J.; Majidi, C.; Schubert, B.; Fearing, R. S. Sliding-induced Adhesion of Stiff Polymer Microfibre Arrays. I. Macroscale Behavior. *J. R. Soc. Interface* **2008**, *5*, 835−844.
(59) Persson, B. N. J. On the Mechanism of Adhesion in Biological Systems. *J. Chem. Phys.* **2003**, *118*, 7614−7621.